THE JOURNAL OF BIOLOGICAL CHEMISTRY VOL. 289, NO. 26, pp. 18214–18227, June 27, 2014

Importance of Mast Cell Prss31/Transmembrane Tryptase/Tryptase-γ in Lung Function and Experimental Chronic Obstructive Pulmonary Disease and Colitis*[S]

Received for publication, January 8, 2014, and in revised form, April 23, 2014 Published, JBC Papers in Press, May 12, 2014, DOI 10.1074/jbc.M114.548594

Philip M. Hansbro[‡1], Matthew J. Hamilton[§1], Michael Fricker[‡], Shaan L. Gellatly[‡], Andrew G. Jarnicki[‡], Dominick Zheng[§], Sandra M. Frei[§], G. William Wong[¶], Sahar Hamadi[§], Saijun Zhou[‖], Paul S. Foster[‡], Steven A. Krilis[‖], and Richard L. Stevens[§2]

From the [‡]Centre for Asthma and Respiratory Disease, University of Newcastle and Hunter Medical Research Institute, Newcastle, New South Wales 2308, Australia, the [§]Department of Medicine, Brigham and Women's Hospital and Harvard Medical School, Boston, Massachusetts 02115, the [¶]Department of Physiology, The Johns Hopkins University School of Medicine, Baltimore, Maryland 21205, and the [‖]Department of Infectious Disease, Immunology, and Sexual Health, St. George Hospital and the University of New South Wales, Kogarah, New South Wales 2217, Australia

Background: Prss31/transmembrane tryptase/tryptase-γ is a mast cell protease.
Results: A Prss31-null mouse was created to evaluate the importance of this enzyme.
Conclusion: Although Prss31 was found to hinder airway reactivity to methacholine, it had pro-inflammatory activity in experimental COPD and colitis.
Significance: These data raise the possibility that human Prss31 has beneficial and adverse roles in the lung and colon.

Protease serine member S31 (Prss31)/transmembrane tryptase/tryptase-γ is a mast cell (MC)-restricted protease of unknown function that is retained on the outer leaflet of the plasma membrane when MCs are activated. We determined the nucleotide sequences of the *Prss31* gene in different mouse strains and then used a Cre/loxP homologous recombination approach to create a novel Prss31$^{-/-}$ C57BL/6 mouse line. The resulting animals exhibited no obvious developmental abnormality, contained normal numbers of granulated MCs in their tissues, and did not compensate for their loss of the membrane tryptase by increasing their expression of other granule proteases. When Prss31-null MCs were activated with a calcium ionophore or by their high affinity IgE receptors, they degranulated in a pattern similar to that of WT MCs. Prss31-null mice had increased baseline airway reactivity to methacholine but markedly reduced experimental chronic obstructive pulmonary disease and colitis, thereby indicating both beneficial and adverse functional roles for the tryptase. In a cigarette smoke-induced model of chronic obstructive pulmonary disease, WT mice had more pulmonary macrophages, higher histopathology scores, and more fibrosis in their small airways than similarly treated Prss31-null mice. In a dextran sodium sulfate-induced acute colitis model, WT mice lost more weight, had higher histopathology scores, and contained more Cxcl-2 and IL-6 mRNA in their colons than similarly treated Prss31-null mice. The accumulated data raise the possibility that inhibitors of this membrane tryptase may provide additional therapeutic benefit in the treatment of humans with these MC-dependent inflammatory diseases.

Mouse mast cells (MCs)[3] store varied combinations of 15 serine proteases in their secretory granules, three of which are the tryptases known as mouse MC protease (mMCP)-6/Tpsb2, mMCP-7/Tpsab1 (1–3), and protease serine member S31 (Prss31)/transmembrane tryptase/tryptase-γ (4). The corresponding *TPSB2*, *TPSAB1*, and *TPSG1/PRSS31* genes expressed in human MCs reside on chromosome 16p13.3. Although the constitutive MCs in the human lung and gastrointestinal tract contain PRSS31 (4, 5), this tryptase is one of the most restricted proteases in the body, and only 15 of the >8.7 million expressed sequence tags (ESTs) in the GenBank™ database originated from its gene (see UniGene Hs.592076).

Although the constitutive safranin^{+} MCs in all examined WT mouse strains express mMCP-6, the corresponding MCs in WT BALB/c and 129/Sv mice have negligible amounts of Prss31 relative to those in C57BL/6 (B6) mice (4). This strain-dependent expression of Prss31 differs from that of mMCP-7, whose gene has a loss-of-function mutation in WT B6 mice (6).

* This work was supported, in whole or in part, by National Institutes of Health Grants DK094971 and AI059746. This work was also supported by the National Health and Medical Research Council of Australia, the Harvard Digestive Diseases Center, the Saint George Medical Research Foundation, and by research fellowship grants from the Harvard Club of Australia Foundation (to S. A. K., R. L. S., P. S. F., and D. Z.).

[S] This article contains supplemental Fig. S1.

The nucleotide sequence(s) reported in this paper has been submitted to the GenBank™/EBI Data Bank with accession number(s) GU810532, GU810531, GU810528, GU810529, and GU810533.

[1] Both authors contributed equally to this work.

[2] To whom correspondence should be addressed: Brigham and Women's Hospital, Dept. of Medicine, Division of Rheumatology, Immunology, and Allergy, Smith Bldg., Rm. 616B, 1 Jimmy Fund Way, Boston, MA 02115. Tel.: 617-525-1231; Fax: 617-525-1310; E-mail: rstevens@rics.bwh.harvard.edu.

[3] The abbreviations used are: MC, mast cell; A1AT, α_1-anti-trypsin; BALF, bronchial alveolar lavage fluid; CAE, chloroacetate esterase; COPD, chronic obstructive pulmonary disease; DSS, dextran sodium sulfate; mBMMC, mouse bone marrow-derived MC; mMCP, mouse MC protease; MMP, matrix metalloproteinase; Prss31, protease serine member S31; B6, C57BL/6; and 6^{+}/7^{-}/31^{-}, mMCP-6$^{+/+}$/mMCP-7−/−/Prss31−/−; qPCR, quantitative PCR.

Mouse Prss31 is initially translated as a 311-mer proteolytically inactive zymogen. Unlike mMCP-6, mMCP-7, and their β-tryptase human orthologs, human and mouse Prss31 has in each instance a membrane-spanning domain near its C terminus that causes the retention of the active form of the enzyme on the outer leaflet of the plasma membrane when MCs degranulate (7). Despite structural differences, recombinant mMCP-6, mMCP-7, human β-tryptases, and human PRSS31 cleave many of the same trypsin-susceptible low molecular weight chromogenic substrates (7, 8). Prss31 therefore has a substrate specificity that overlaps that of its tetramer-forming family members. Although the function of Prss31 is not known, the tetramer-forming tryptases mMCP-6 and mMCP-7 have prominent beneficial roles in innate immunity (9–11) but substantial adverse roles in numerous inflammatory diseases (12–14).

We recently developed a novel cigarette smoke-induced 8-week model of COPD in mice that is dependent on pulmonary macrophages and mMCP-6^+ MCs (14) to advance our knowledge of this devastating disease. A serine protease·protease inhibitor imbalance in the lung is a major risk factor in COPD (15), and humans that are deficient in α_1-antitrypsin (A1AT)/SERPINA1 (16) or α_2-macroglobulin (17) are at increased risk of developing emphysema. Other than neutrophil elastase, the relevant A1AT-susceptible serine proteases in human lung that increase the risk of developing emphysema and pulmonary inflammation have not been identified. Macrophage accumulation, alveolar enlargement, and varied aspects of lung function were not reduced significantly in our smoke-treated WT mice that were depleted of their neutrophils (14). We therefore hypothesized that an A1AT-regulated proinflammatory serine protease other than neutrophil elastase probably has a prominent adverse role in this pulmonary disease. We also speculated that this enzyme would have tryptic activity because A1AT inhibits such serine proteases. In this regard, we previously showed that recombinant Prss31 is rapidly inhibited by A1AT *in vitro* (7).

Because tryptase redundancy occurs in some inflammatory disease models (12), we concluded that we probably would need to delete at least two of the three MC-restricted tryptases in mice to uncover the global importance of this family of serine proteases in experimental COPD, colitis, and other inflammatory disease models.

The adoptive transfer of *in vitro*-differentiated mMCP-6^+/mMCP-7^+ MCs from WBB6F_1/J-+/+ mice into MC-deficient WBB6F_1/J-*Kit*^{W}/*Kit*$^{W\text{-}v}$ mice provided insights into the function of MCs and their tetramer-forming tryptases in varied experimental models (18). Unfortunately, because the MCs in WBB6F_1/J-*Kit*^{W}/*Kit*$^{W\text{-}v}$ mice constitutively contain low amounts of Prss31 (19), this reconstitution approach cannot be used to evaluate the importance of the latter membrane tryptase *in vivo*. To deal with that obstacle, we created in this study a novel inbred transgenic mMCP-$6^{+/+}$/mMCP-$7^{-/-}$/Prss31$^{-/-}$ ($6^+/7^-/31^-$) B6 mouse line in which the functional *Prss31* gene was ablated in mMCP-7-null B6 mouse ES cells. Using this transgenic mouse, we discovered that Prss31 has beneficial roles in hindering airway reactivity to methacholine but prominent adverse roles in experimental COPD and colitis.

EXPERIMENTAL PROCEDURES

All experiments were carried out using animal protocols approved by the Brigham and Women's Hospital/Dana Farber Cancer Institute or the University of Newcastle animal ethics committees.

Sequence Analysis of the Prss31 Genes in Different WT Mouse Strains—Purified A/J, BALB/c, CBA, C3H/HeJ, and SWR mouse genomic DNA were obtained from The Jackson Laboratory (Bar Harbor, ME), and a standard PCR approach was used to isolate the entire 3.9-kb *Prss31* gene from the five WT mouse strains employing primers that resided at the beginning (5′-cccatactgataggcctggggctggg-3′) and end (5′-atttgctttatgtcatccgttctac-3′) of the tryptase gene. The resulting 3.9-kb genomic fragments were purified and sequenced in both directions using seven forward and seven reverse primers spaced every 500–600 nucleotides based on the sequence of the 129/Sv mouse *Prss31* gene (4).

Creation of a Novel Transgenic $6^+/7^-/31^-$ B6 Mouse Line—Exon 1 of the endogenous 3.9-kb mouse *Prss31* gene encodes the translation-initiation site of the expressed transcript and the hydrophobic signal peptide of the translated tryptase (4). Thus, no functional Prss31 protein can be produced in mice if this exon is removed using a Cre/loxP homologous recombination approach. Another reason why the first exon of the *Prss31* gene was targeted was because the last 156 nucleotides of its fifth exon are shared with that of the *Cacna1h* gene. Cacna1h is a calcium channel protein important in brain and heart development, and mutations in the human *CACNA1H* gene lead to epilepsy and autism spectrum disorders (20). Transgenic mice lacking just the sixth exon of the latter gene (causing loss of amino acids 216–267 in this 2007-mer protein) have constricted coronary arterioles and focal myocardial fibrosis (21). We therefore concluded that targeted removal of the 3′ end of the mouse *Prss31* gene most likely would adversely affect the expression of the physically linked *Cacna1h* gene which, in turn, would almost certainly lead to serious developmental abnormalities in the resulting transgenic mice.

The Prss31-targeting vector employed to create the transgenic mouse line used in this study was generated with the assistance of Taconic-Artemis using BAC clones from their B6 mouse RPCIB-731 BAC library. A loxP site was placed 1.9 kb upstream of the gene's first exon. The second loxP site was placed in the gene's first intron. The puromycin resistance (*PuroR*) gene flanked by F3 sites was inserted into intron 1 upstream of the second loxP site for positive selection, whereas the thymidine kinase (*Tk*) gene was inserted upstream of the *mMCP-6/Tpsb2* gene for negative selection. The B6 mouse ES cell line was grown on a mitotically inactivated feeder layer of mouse embryonic fibroblasts in DMEM high glucose medium supplemented with 20% FBS and 1,200 units/ml leukemia inhibitory factor (Millipore ESG 1107). Thirty μg of the linearized targeting DNA were electroporated into 10^6 ES cells using a Gene Pulser (Bio-Rad) at 240 V and 500 microfarads. Puromycin (1 μg/ml) and gancyclovir (2 μM) positive and negative selection treatments were commenced on days 2 and 5, respectively. The resulting transfectants were isolated and analyzed on day 8.

Assessed by DNA blot and/or qPCR analysis, 17 of the obtained 252 ES cell clones had undergone homologous recombination at the *Prss31* genomic locus, as shown for clone C1. After the transfer of this clone into mouse blastocysts, chimera $Prss31^{f/+}$.FLpe mice were obtained that had one allele of the mouse *Prss31* gene floxed. After Flp-mediated removal of the *PuroR* gene, the obtained $Prss31^{f/+}$ heterozygote mice were mated. The identified $Prss31^{f/f}$ offspring containing both alleles of the *Prss31* gene floxed were next bred with Taconic-Artemis's CreDel mouse B/6-Gt(ROSA)26Sor$^{tm9(cre/ESR1)Arte}$. The resulting $Prss31^{-/+}$.CreDel offspring were mated with WT B6 mice to obtain $Prss31^{-/+}$ B6 mice that had one WT allele and one disrupted allele of the targeted gene. These heterozygotes were bred to obtain the final $Prss31^{-/-}$ B6 mouse line that contained both disrupted alleles of the *Prss31* gene.

A standard PCR approach was carried out to genotype our $Prss31^{+/+}$, $Prss31^{+/-}$, and $Prss31^{-/-}$ B6 mice in which genomic DNA isolated from proteinase K-digested tails was incubated with the primers 5′-ctgttcattccctgtttgttgg-3′ and 5′-cctgaggtagatgttcccatcc-3′. After an initial denaturation step (94 °C for 10 min), 35 cycles of PCR were carried out with denaturation (94 °C for 15 s), annealing (55 °C for 30 s), and extension (72 °C for 70 s) steps. Because the MCs in WT B6 mice cannot express mMCP-7 due to a splice-site mutation in its gene (6, 22), the MCs in the created B6 mouse line lack both mMCP-7 and Prss31.

Histochemistry and Enzyme Cytochemistry Evaluation of the MCs in the Peritoneum and Ear of the Prss31-null Mouse—To examine the *in vivo*-differentiated MCs in the peritoneal cavity, WT and Prss31-null B6 mice were euthanized with CO_2. Ten ml of PBS was injected into the peritoneal cavity of each animal and then aspirated ~10 s later. The resulting lavage fluid was centrifuged at 450 × *g* for 5 min, and the obtained cell pellet in each instance was resuspended in 0.5 ml of PBS. One hundred-μl samples were cytocentrifuged onto glass slides that were then stained with toluidine blue or with Alcian blue followed by safranin (23) to evaluate the number of MCs and their overall granulation, as well as their expression and granule accumulation of heparin-containing serglycin proteoglycans. To examine the constitutive MCs in Prss31-null B6 mice, the left and right ears were harvested and placed overnight in 4% paraformaldehyde. The fixed tissues were cut, embedded in paraffin, and sectioned, and the resulting slides were subjected to H&E histochemistry or chloroacetate esterase enzyme (CAE) cytochemistry (24).

Generation and Characterization of Prss31-null B6 Mouse Bone Marrow-derived MCs (mBMMCs)—After euthanasia with CO_2, harvested bone marrow cells from the femora and tibiae of WT and Prss31-null B6 mice were cultured for >4 weeks in IL-3-enriched WEHI-3 cell-conditioned medium, as described previously (25). In two experiments to evaluate the IL-10 signaling pathway in Prss31-null MCs, the two populations of IL-3-developed mBMMCs were exposed to 10 ng/ml recombinant IL-10 (R&D Systems) for 24 h, as described previously (26).

Based on our earlier analyses of the protease composition of the MCs in WT $6^+/7^+/31^-$ BALB/c and WT $6^+/7^-/31^+$ B6 mice, the expression and granule accumulation of the other proteases in the cell's secretory granules are not dependent on Prss31. Nevertheless, RT-qPCR approaches were used to confirm that targeted inactivation of the *Prss31* gene in our newly created $6^+/7^-/31^-$ B6 mouse line did not cause the MCs in these animals to increase their expression of another granule protease. For these experiments, WT and Prss31-null B6 mBMMCs were centrifuged, and the resulting cell pellets were placed in Qiagen's cell lysis buffer. Each lysate was applied to an RNeasy spin column using the manufacturer's recommended protocols. Once RNA was isolated and quantitated spectrophotometrically, the iScript cDNA synthesis kit (Bio-Rad) was used to convert comparable amounts of the RNA from each sample into cDNA.

The obtained cDNA samples were analyzed by RT-qPCR using a Stratagene Mx3000P PCR machine, a SYBR Green PCR kit (Bio-Rad), and validated primers specific for the transcripts that encode GAPDH, serglycin, carboxypeptidase A3, mMCP-1, mMCP-2, mMCP-4, mMCP-5, mMCP-6, and Prss31 (Qiagen). The obtained data for each transcript were then normalized based on the level of the GAPDH transcript in each sample.

The mMCP-4, mMCP-5, and mMCP-6 mRNA data in IL-3-developed mBMMCs were confirmed and extended by SDS-PAGE immunoblot analysis using the relevant mMCP-specific anti-peptide antibodies generated in rabbits. For these experiments, *in vitro*-developed Prss31-null mBMMCs and *in vivo*-developed peritoneal MCs from the Prss31-null B6 mice were placed in ice-cold PBS and sonicated in a cold room for ~5 s. SDS-PAGE buffer (2×) was quickly added, and the resulting lysates were boiled for 5 min to minimize proteolysis of the liberated cell's granule proteins. The resulting lysates were loaded onto 12% acrylamide gels (Bio-Rad). After a 90-min electrophoresis at 90 V, each gel was transferred overnight onto a polyvinylidene difluoride membrane (Millipore) at 4 °C and at 35 V. The resulting blots were blocked with a 5% solution of nonfat dry milk in TBS for 1 h, and then washed with 0.02% Tween 20 in TBS. The treated blots were next incubated for 1 h with 1:200–1,000-fold dilutions of affinity-purified anti-mMCP-4 (27), anti-mMCP-5 (28), or anti-mMCP-6 (26) IgG. The immunoblots were washed, incubated for 1 h with horseradish peroxidase-labeled goat anti-rabbit IgG (Bio-Rad), and washed again. The membranes were developed with blot detection reagents (GE Healthcare) in a 1:1 ratio for 1 min, and then exposed in a dark room for 10–60 s.

Activation of mBMMCs and Release of the Cell's Granule Constituents and Newly Generated TNF-α—WT mBMMCs can be induced to degranulate and release β-hexosaminidase and numerous cytokines and chemokines when exposed to calcium ionophore A23187 or IgE followed by antigen. Because Prss31 resides in the secretory granules of MCs, this membrane tryptase only becomes available to affect bystander cells in the lung and gastrointestinal tract when MCs degranulate (7). After MCs exocytose their preformed mediators, they then increase their expression and release of TNF-α and many other cytokines and chemokines (29). The ability of MCs to degranulate and release their varied families of mediators in response to calcium ionophore and IgE/antigen signaling was therefore evaluated.

For these experiments, WT and Prss31-null B6 mBMMCs (2×10^5 cells/ml) were placed in 200 μl of Tyrode's buffer containing 1% dimethyl sulfoxide with or without 4 μM calcium ionophore A23187 (Sigma) for 30 min, as done in earlier studies (30). The activated mBMMCs were centrifuged, and the supernatants and cell pellets were collected. The pelleted cells were resuspended in Tyrode's buffer and sonicated.

For FcεRI-dependent activation, WT and Prss31-null B6 mBMMCs were placed in 10 ml of fresh culture medium (1×10^6 cells/ml) supplemented with 0.3 μg/ml anti-trinitrophenyl-IgE. After an overnight incubation at 37 °C, 1.5 ml of each cell suspension was placed in a 2.0-ml centrifuge tube, centrifuged, and washed once with HBSS. The IgE-sensitized mBMMCs were resuspended in 200 μl of fresh Tyrode's buffer with or without trinitrophenyl-BSA (10 ng/ml), and the treated cell suspensions were incubated for 30 min at 37 °C. The FcεRI-activated mBMMCs were once again centrifuged, and the supernatants and cell pellets were collected. The cell pellets were resuspended in Tyrode's buffer and sonicated.

The chromogenic assay developed by Robinson and Stirling (31) was used to measure the calcium ionophore- and FcεRI-mediated net percent releases of the granule constituent β-hexosaminidase. For evaluation of the FcεRI-dependent expression of TNF-α protein, replicate IgE-sensitized WT and Prss31-null mBMMCs were exposed to the relevant antigen for 90 min. The resulting supernatants were harvested, and the levels of the cytokine were determined using an ELISA kit from eBioscience.

Baseline Blood Cell Populations—WT and Prss31-null B6 mice were sacrificed by an overdose of sodium pentobarbital, followed by cardiac puncture. In each instance, a single drop of blood was smeared onto a microscope glass slide, which was then stained with H&E. The differential cell populations were enumerated based on their morphology, as described previously (32).

Lung Function before and after Exposure to Methacholine—WT and Prss31-null B6 mice were anesthetized and cannulated for invasive plethysmography. Forced maneuver methods were used to measure lung capacity (namely total lung, inspiratory, and functional residual capacity), and forced oscillation techniques were used to assess lung function (namely transpulmonary and airway-specific resistance and compliance, dynamic elastance, inertance, and tissue damping) before and after the animals were exposed to methacholine (between 0 and 10 mg/ml in 15 μl of PBS) via nebulization. Lung measurements were taken shortly after the mice were exposed to methacholine. All of these methods have been described previously (14, 33, 34).

Cigarette Smoke-induced Experimental COPD—The conditions used to induce and then gauge experimental COPD in WT and Prss31-null B6 mice treated with cigarette smoke for 8 weeks have been described (14). Briefly, nose-only exposure was used to deliver cigarette smoke into the lungs of each animal for 1 h twice a day, 5 days/week for 8 weeks. Each day, program-controlled 30-s breaks were interspersed with 30-s puffs of smoke to mimic human smoking. This regime roughly equates to a human smoking one pack of cigarettes per day, as we described recently (35). Age-matched control WT and Prss31-null B6 mice breathed normal air continually for 8 weeks. Airway inflammation was determined by collection of the bronchoalveolar lavage fluid and enumeration of the inflammatory cells based on their morphology at week 8. Lungs were perfused, inflated, embedded in paraffin, and sectioned. Parenchymal inflammation was assessed by counting the number of inflammatory cells in 10 randomized fields of H&E-stained lung sections.

Pulmonary fibrosis was visualized histochemically in formalin-fixed lung tissue sections using a Verhoeff-Van Gieson staining kit. Sections of lung on glass slides were sequentially stained in Verhoeff's solution for 1 h, rinsed with tap water, immersed in 2% ferric chloride for 2 min, rinsed in tap water, immersed in 5% sodium thiosulfate for 1 min, rinsed in tap water, and immersed in Van Gieson's solution for 5 min. After the slides were dried, they were mounted in Entellan medium. The area of fibrosis (stained bright pink) surrounding small airways was quantified for at least four airways/section. All measurements were made using ImageJ software, and quantification was expressed as the area of fibrosis (μm^2) divided by the perimeter (μm) of the basement membrane of the evaluated small airway ($\mu m^2/\mu m$). Small airways were defined as having a basement membrane perimeter of $\leq$1,000 μm.

Experimental Acute Colitis—For these experiments, 8–10-week-old male and sibling WT and Prss31-null B6 mice were used with presumably similar intestinal microbiomes. Employing a previously developed experimental protocol (13, 36), the two groups of animals were exposed to dextran sodium sulfate (DSS) (36–50 kDa; MP Biomedicals) at a concentration of 2.0% in their drinking water for 5 days. On days 6 and 7, the treated mice were given normal drinking water. Exposure of WT B6 mice to these experimental conditions results in substantial inflammation and a 7–15% weight loss without mortality (13).

After the DSS-treated mice were sacrificed at day 7, their colons were harvested from terminal ileum to distal rectum, measured in length, and processed for H&E histochemistry. A 20-point scoring system was used to assess the degree of colitis (13, 37). For quantitating the levels of specific transcripts in the affected colon, ~1-cm sections of distal colons were resected and placed into RNAlater (Ambion) at 4 °C overnight to inactivate RNases. The treated tissue samples were homogenized and washed in PBS, and their RNA was purified in each instance using an RNeasy column (Qiagen). Once the isolated RNA was converted to cDNA, the transcripts that encode GAPDH, IL-6, Cxcl-1, Cxcl-2, and matrix metalloproteinase (Mmp)-13 were quantified by RT-qPCR using Qiagen's validated primer sets since we showed previously that these cytokine, chemokine, and MMP transcripts are induced in DSS-treated B6 mice (13).

Statistical Analyses—The obtained data were analyzed using GraphPad Prism software (version 6.00). The airway methacholine reactivity data were analyzed by the two-way analysis of variance with Dunnett's multiple comparison test. The COPD data were analyzed by one-way analysis of variance with post hoc Tukey's test. The Student's unpaired *t* test was performed on the colitis data to evaluate means ± S.E. to compare differences between WT and Prss31-null B6 mice with regard to the blood cell type, weight change, colon length, histopathology

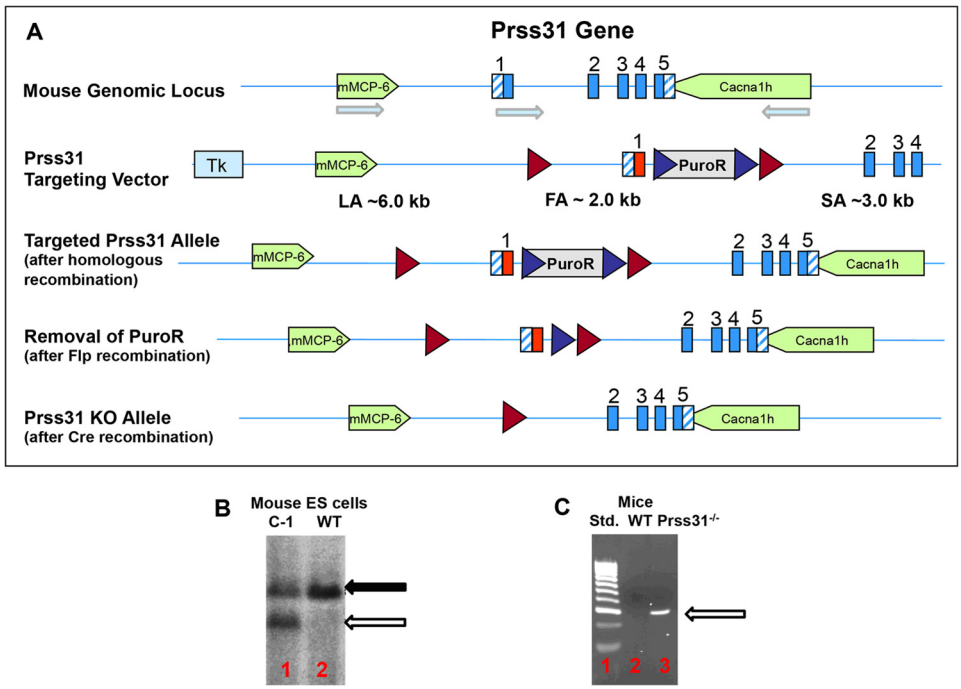

FIGURE 1. **Creation of a transgenic Prss31-null B6 mouse.** *A–C,* shown in *A* is the genomic locus that contains the B6 mouse *Prss31* gene and its upstream *mMCP-6/Tpsb2* and downstream *Cacna1h* genes. Also shown in this panel is the Prss31-targeting vector with its loxP (*red* ◭) and F3 (*blue* ◭) sites and the coding (*solid blue*) and untranslated (*hatched blue*) portions of the exons of the mouse *Prss31* gene. The *arrows* indicate the orientations of the *mMCP-6*, *Prss31*, and *Cacna1h* genes on mouse chromosome 17A3.3. The sizes and locations of the long (*LA*), floxed (*FA*), and short (*SA*) arms of homology are shown. After homologous recombination, the negative selection marker Tk is lost, and the nucleotide sequence of the targeting vector has replaced one of the alleles of the endogenous *Prss31* gene in the B6 mouse ES cells. To demonstrate that homologous recombination took place in the C1 ES cell clone that was injected into mouse blastocysts (*B*), genomic DNA was isolated from this clone and from untreated ES cells. In both instances, the resulting DNA was digested with the restricted enzyme NsiI and subjected to gel electrophoresis. The resulting DNA blot was then probed with a genomic fragment residing upstream of the normal mouse *Prss31* gene. Because an NsiI-susceptible sequence resides just after the first loxP site in the targeting vector, a smaller genomic fragment (*open arrow, lane 1*) than the WT *Prss31* gene (*solid arrow, lanes 1* and *2*) is obtained if homologous recombination takes place at one of the alleles of the mouse *Prss31* gene. The DNA blot was next analyzed with a PuroR probe to confirm the presence of the positive selection marker. Once chimeras and heterozygotes were generated, Flp-mediated recombination was used to remove the positive selection marker PuroR. Cre-mediated recombination was then employed to remove the first exon of the *Prss31* gene. Heterozygotes containing one WT and one disrupted allele of the *Prss31* gene were bred to create the final Prss31-null B6 mouse line (*C, lane 3*). Standard molecular weight 100-bp markers are shown in *C, lane 1*. The relevant DNA product (*C, lane 3*) identified in the confirmatory PCR-based genotyping approach we used is 326 bp. The entire process to create the final mouse line took >4 years of effort.

score, and RT-qPCR data. Probability (p) values <0.05 were considered statistically significant.

RESULTS

Nucleotide Sequence Analysis of the Prss31 Gene in Different Mouse Strains—The nucleotide sequences of the A/J, BALB/c, CBA, C3H/HeJ, and SWR mouse *Prss31* genes were determined to ensure that there was nothing abnormal about the B6 mouse *Prss31* gene and its translated product, as well as to determine whether it was better to inactivate the *Prss31* gene in B6, 129/Sv, or BALB/c mouse ES cells. The deduced nucleotide sequences of the tryptase gene in the five mouse strains (as well as the previously determined 129/Sv mouse strain (4)) are compared in supplemental Fig. S1 with that of the corresponding B6 mouse gene. Although 40 nucleotides were different in the *Prss31* genes in the genomes of BALB/c and B6 mice in this head-to-head comparison, nearly all of these allelic variations resided in their introns. One nucleotide difference in exon 1 resulted in a Tyr-6/Asn-6 change in the signal peptide of the translated zymogen. Because the signal peptide of translated human PRSS31 lacks both amino acids (4), the Tyr-6/Asn-6 allelic difference in mouse Prss31 most likely does not affect the ability of the mouse MC to remove the signal peptide of the initially translated zymogen in the cell's endoplasmic reticulum. Based on the nucleotide sequences of the gene's remaining exons, the propeptides and catalytic domains of B6, 129/Sv, A/J, BALB/c, CBA, C3H/HeJ, and SWR mouse Prss31 are identical.

Creation of a Prss31-null B6 Mouse—Because the tissue expression pattern of the Prss31 transcript in the WT B6 mouse is similar to that of the human PRSS31 transcript (4) (also see the expressed sequence tag data at GenBank™ UniGene Hs.592076 and Mm.180108), we hypothesized that this mouse strain could be used to obtain valuable insight as to the function of its human ortholog. A transgenic $6^+/7^-/31^-$ B6 mouse line (Fig. 1) therefore was created using the homologous recombination and animal mating approaches described under "Experimental Procedures." The resulting Prss31-null B6 mice were viable and had no obvious developmental abnormality. They also had a normal life span.

The constitutive MCs in the connective tissues of WT B6 mice express Prss31, and the histology of every examined organ in the $6^+/7^-/31^-$ B6 mouse line was grossly normal, as shown for the ear (Fig. 2, *A* and *C*). When WT $6^+/7^-/31^+$ and transgenic $6^+/7^-/31^-$ B6 mice were compared, there was no significant difference in the number of MCs in the ear (11.0 ± 0.7 *versus* 10.5 ± 0.5 MCs/high power fields for 10 examined high power fields for two mice for each strain) or peritoneal cavity

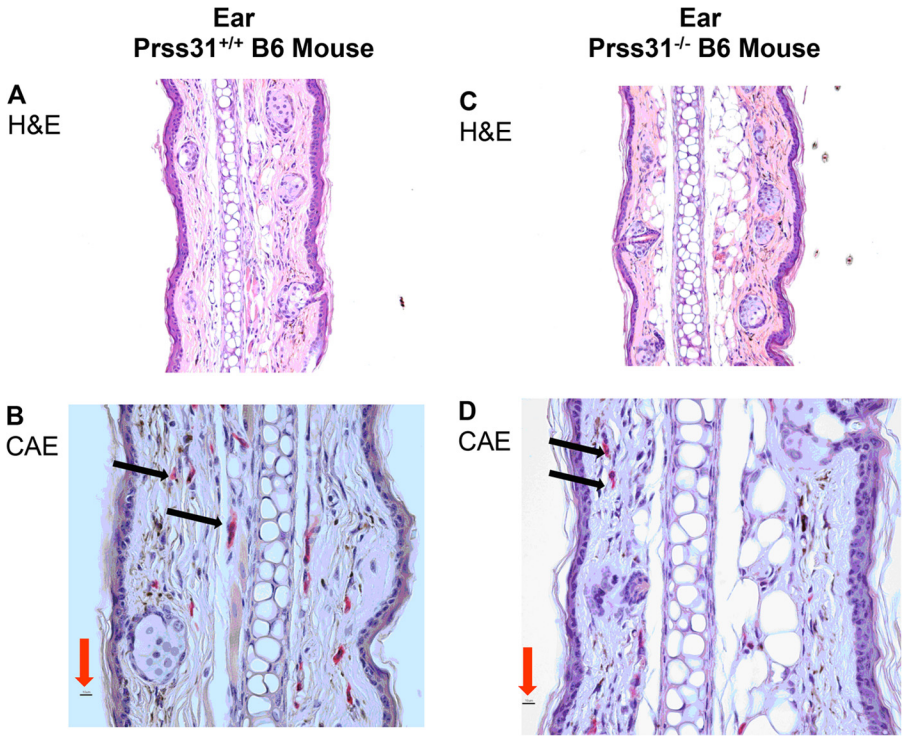

FIGURE 2. **Histochemistry and enzyme cytochemistry of the cutaneous MCs in WT and Prss31-null B6 mice.** *A–D*, identification of CAE^+ cutaneous MCs. Sections of the ears of WT (*A* and *B*) and Prss31-null (*C* and *D*) mice were subjected to H&E histochemistry (*A* and *C*) and enzyme cytochemistry (*B* and *D*). No ultrastructural abnormality was detected in the ears of the Prss31-null mice, as also occurred in the jejunum (data not shown). All MCs in WT B6 mice are CAE^+ due to their granule storage of large amounts of the chromosome 14C3 family members mMCPs 1–5 and 8–10. WT and Prss31-null B6 mice constitutively had similar numbers of CAE^+ MCs (*red* cells highlighted by *black arrows*) in their ears (*B* and *D*). Thus, Prss31 is not essential for the recruitment of MC-committed progenitors into the ear or for their development into mature MCs, as anticipated. For size comparison, the *red arrows* in *B* and *D* point to the 10-μm magnification bars.

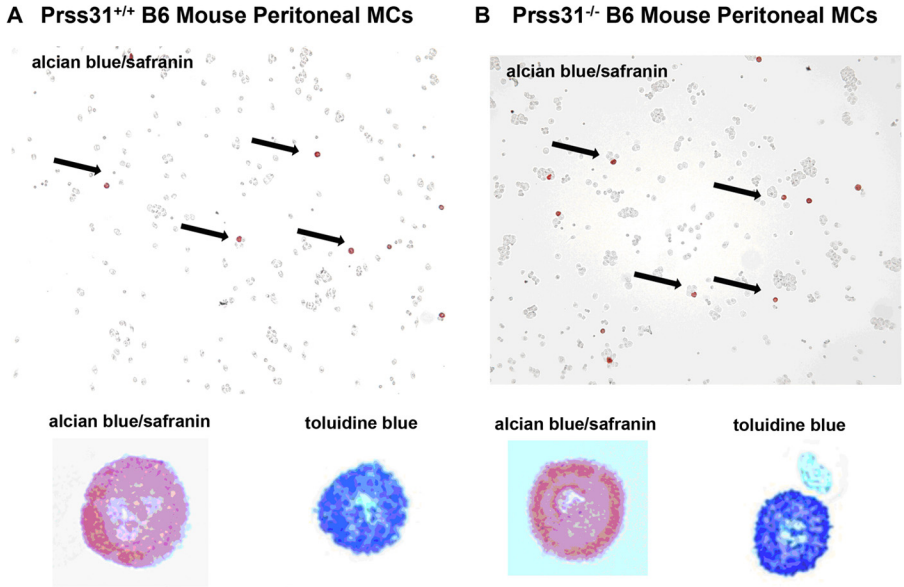

FIGURE 3. **Histochemistry of the peritoneal MCs in WT and Prss31-null B6 mice.** *A* and *B*, peritoneal lavage was performed on WT (*A*) and Prss31-null (*B*) B6 mice. Cytospins of the cells in the resulting exudates were stained with toluidine blue or with Alcian blue followed by safranin. Shown at lower power (highlighted by *black arrows*) and at higher power in the *bottom left insets* are the $safranin^+$ MCs in the exudates. Shown at higher power in the *bottom right insets* are the corresponding peritoneal MCs in these exudates stained with toluidine blue. Toluidine blue recognizes all types of negatively charged serglycin proteoglycans in the granules of MCs, including those that contain chondroitin sulfate diB, chondroitin sulfate E, and heparin glycosaminoglycans. In contrast, safranin preferentially recognizes those serglycin proteoglycans that contain heparin glycosaminoglycans. The relative numbers of $safranin^+$ and $toluidine\ blue^+$ MCs in the peritoneal cavities of the two mouse strains were the same, as were their degree of granulation and expression of heparin-containing serglycin proteoglycans.

(3.1 ± 0.5 *versus* 4.0 ± 0.3 MCs/100 total cells in the exudates of two mice for each strain). In addition, there was no noticeable difference in the histochemical appearance of the MCs in the ear (Fig. 2, *B* and *D*) and peritoneal cavity (Fig. 3).

The cytokine receptors Kit/CD117 and ST-2/IL1RL1 and their respective ligands KitL/stem cell factor and interleukin (IL)-33 are essential for the development of the MCs in the skin and other tissues of mice. Thus, the observation that Prss31-

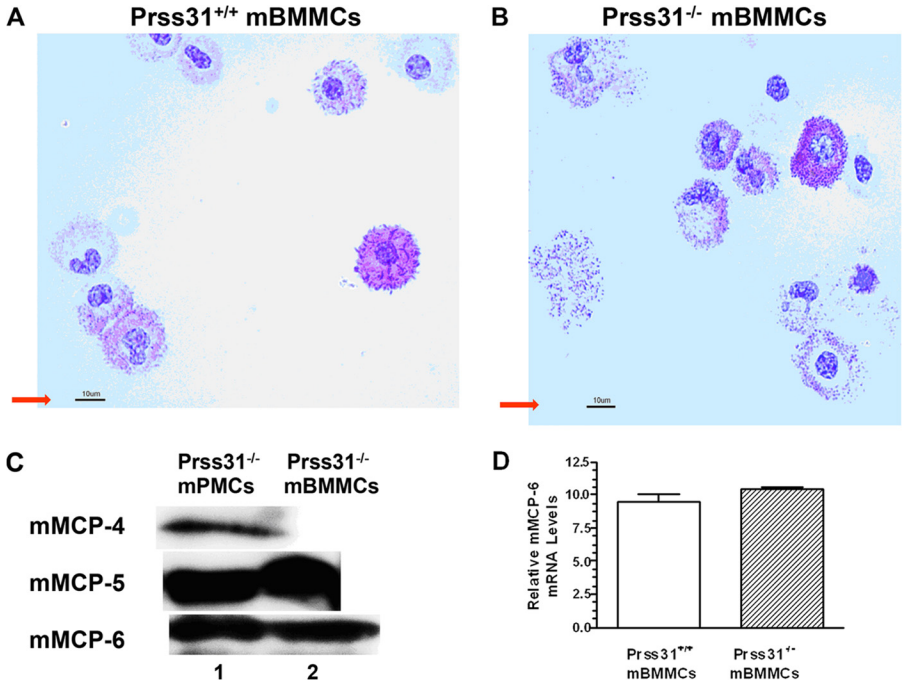

FIGURE 4. **Histochemistry of WT and Prss31-null mBMMCs and protease expression in mBMMCs and peritoneal MCs.** *A* and *B,* bone marrow cells harvested from WT (*A*) and Prss31-null (*B*) B6 mice were cultured for >4 weeks in the presence of IL-3-enriched WEHI-3 cell conditioned medium. As found in earlier studies (25), the resulting mBMMCs generated from WT B6 mice varied considerably in their degree of granule maturation (*A*). Nevertheless, because similar numbers of histochemically identical mBMMCs were generated from Prss31-null B6 mice (*B*), there was no defect in the IL-3/IL3Rα signaling pathways in MCs developed from Prss31-null mice. For size comparison, the *red arrow* pointing to the 10-μm magnification bar is shown in each panel. *C,* levels of mMCP-4, mMCP-5, and mMCP-6 protein in lysates of *in vivo*-differentiated Prss31-null mouse peritoneal MCs (*mPMCs*) and *in vitro*-differentiated Prss31-null mBMMCs were determined by SDS-PAGE immunoblot analyses. Lysates of the two populations of MCs were subjected to SDS-PAGE, and the resulting protein blots were stained with affinity-purified anti-peptide antibodies that recognize mMCP-4, mMCP-5, and mMCP-6. As found previously for WT B6 mice (1, 41) and in agreement with the histochemistry and CEA enzyme cytochemistry, mouse peritoneal MCs isolated from Prss31-null mice (*lane 1*) stored substantial amounts of all three serine proteases in their secretory granules, whereas the levels of mMCP-4 protein were below detection in IL-3-developed mBMMCs (*lane 2*). *D*, because the *mMCP-6* gene resides immediately upstream of the *Prss31* gene (Fig. 1), the level of the mMCP-6 transcript was quantitated in WT and Prss31-null B6 mBMMCs. Shown are the relative *Ct* expression levels of the mMCP-6 transcript normalized to that of the GAPDH transcript (mean ± ½ range, $n = 2$). Similar RNA data were obtained in a second experiment also carried out using mBMMCs obtained from two WT B6 mice and two Prss31-null mice. In agreement with the SDS-PAGE immunoblot data (*C*), targeted inactivation of the *Prss31* gene using our Cre/loxP homologous recombination approach did not adversely affect transcription of the nearby *mMCP-6* gene in IL-3-developed mBMMCs.

null B6 mice contained normal numbers of mature MCs in their skin and peritoneal cavity indicated that Kit/KitL- and IL-33/IL1RL1-signaling pathways were functional in the MCs of Prss31-null mice.

Analysis of Prss31-null mBMMCs—As in WT B6 mice, immature mBMMCs could be generated by culturing the bone marrow cells from Prss31-null B6 mice in IL-3-enriched medium (Fig. 4, *A* and *B*). Thus, critical IL-3/IL3Rα signaling pathways also were intact in Prss31-null B6 mBMMCs.

Because the mouse *Prss31* gene resides only 2.3 kb downstream of the *mMCP-6* gene (Fig. 1), our biggest concern was that targeted inactivation of the *Prss31* gene using our Cre/loxP homologous recombination approach could lead to a positional defect on chromosome 17A3.3, which indirectly caused a failure of the MCs in the newly created Prss31-null mice to transcribe the *mMCP-6* gene. The SDS-PAGE immunoblot data shown in Fig. 4*C* revealed that the peritoneal MCs in Prss31-null mice and the mBMMCs developed from these transgenic mice contained substantial amounts of mMCP-6 protein, as well as mMCP-5 protein for both populations of MCs and additionally mMCP-4 protein for peritoneal MCs. In confirmation of these SDS-PAGE immunoblot data, there was no significant difference in the levels of the mMCP-6 transcript in the IL-3-developed mBMMCs from WT and Prss31-null B6 mice (Fig. 4*D*). Likewise, the levels of the transcripts that encode mMCP-5, serglycin proteoglycan, and carboxypeptidase A3 were all abundant in Prss31-null mBMMCs, as assessed by RT-qPCR analyses.

Although IL-3-developed WT B6 mBMMCs contain high levels of the transcripts that encode four MC-restricted proteases, we previously showed that these pluripotent immature MCs constitutively contain low levels of the transcripts that encode mMCP-1, mMCP-2, and mMCP-4 due to a post-transcriptional pathway that catabolizes these three protease transcripts as fast as they are produced in IL-3-developed mBMMCs. As assessed by RT-qPCR analysis, the levels of the mMCP-1, mMCP-2, and mMCP-4 transcripts were nearly below detection in IL-3-developed mBMMCs from Prss31-null mice. However, like WT mBMMCs, these Prss31-null mBMMCs increased their levels of the mMCP-1 and mMCP-2 transcripts >20-fold over that in untreated mBMMCs (but not their levels of mMCP-5) when exposed to IL-10 for 24 h (Fig. 5). The latter data indicated that IL-10-dependent signaling pathways were functional in Prss31-null mouse MCs.

Finally, when activated with calcium ionophore A23187 or via their high affinity IgE receptors, WT and Prss31-null mBMMCs released similar amounts of β-hexosaminidase and generated similar amounts of TNF-α (data not shown). Thus,

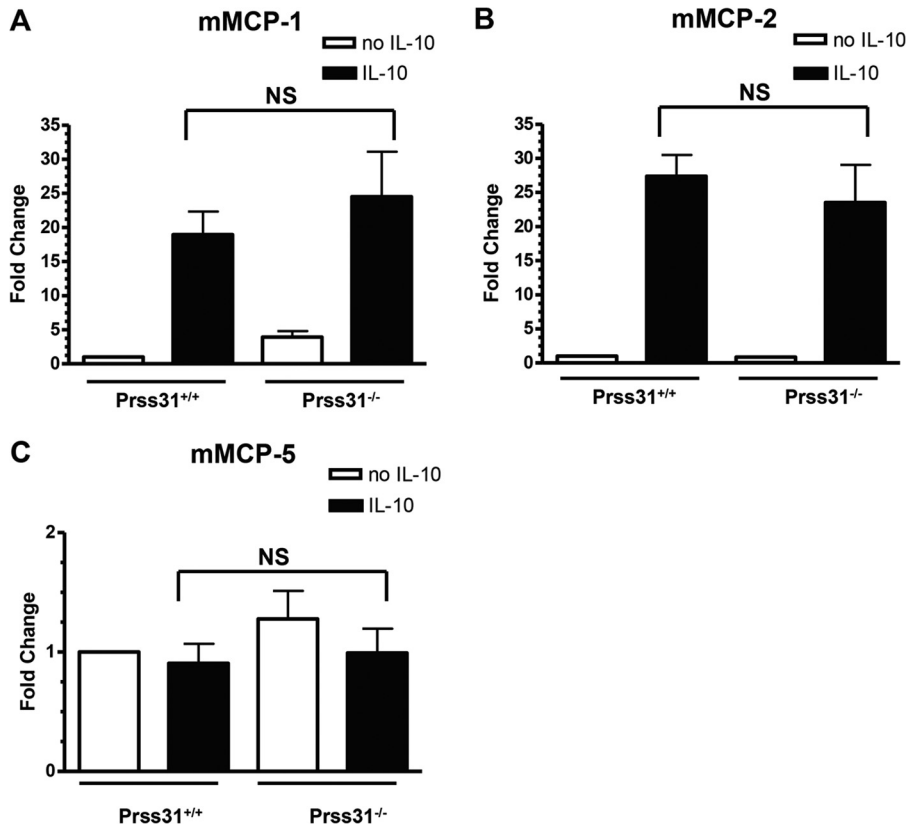

FIGURE 5. **IL-10 induces the expression of mMCP-1 and mMCP-2 in WT and Prss31-null mBMMCs.** *A–C*, WT $6^+/7^-/31^+$ and transgenic $6^+/7^-/31^-$ B6 mBMMCs were cultured in the presence (■) or absence (□) of IL-10 ($n = 3$/group) for 24 h. In each instance, RNA was isolated and converted to cDNA, and the levels of the transcripts that encode mMCP-1 (*A*), mMCP-2 (*B*), and mMCP-5 (*C*) were determined. The obtained data were then normalized to that of the ubiquitously expressed GAPDH transcript. Results were expressed as fold-change differences relative to that in replicate mBMMCs that had not been exposed to IL-10. As occurred in WT mBMMCs, Prss31-null mBMMCs markedly increased their levels of mMCP-1 and mMCP-2 mRNA when exposed to IL-10. In contrast, the levels of the mMCP-5 transcript were not significantly (*NS*) different. Similar findings were obtained in a second experiment, also carried out in triplicate.

the calcium ionophore- and FcεRI-signaling pathways in these MCs also were functional.

Baseline Blood Cell Populations and Lung Function in Naive Prss31-null Mice before and after Exposure to Methacholine—As assessed histochemically, no significant differences were found in the numbers of monocytes, neutrophils, or lymphocytes in the blood of untreated WT and Prss31-null mice (Fig. 6*A*). The possible role of Prss31 in the maintenance of lung function in naive mice before and after methacholine challenge was next evaluated (Fig. 6, *B–H*). No differences were found in baseline functional residual, total lung inspiratory, or vital capacity in Prss31-null B6 mice compared with WT B6 mice. There also were no differences in baseline transpulmonary or airway resistance, dynamic compliance or elastance, inertance, or tissue damping. In contrast, when challenged with methacholine (Fig. 6, *B–H*), Prss31-null mice had increased airway resistance, transpulmonary resistance, hysteresivity, dynamic elastance, tissue elastance, and tissue damping but decreased dynamic compliance relative to similarly treated WT B6 mice.

Cigarette Smoke-induced Experimental COPD—mMCP-6 plays prominent roles in cigarette smoke-induced COPD (14). Thus, whether or not Prss31 also contributes to this experimental model was investigated. As found in our previous study carried out on WT and mMCP-6-null B6 mice (14), the numbers of leukocytes in the bronchial alveolar lavage fluid (BALF) of smoke-treated WT B6 mice were significantly greater than that of control WT B6 animals, which breathed normal room air (Fig. 7*A*). In support of these data, the numbers of peribronchial, perivascular, and parenchymal inflammatory cells were substantially increased in the lungs of smoke-treated WT B6 mice (Fig. 7, *C* and *D*). This cellular increase was markedly attenuated in smoke-treated Prss31-null mice.

Differential cell counts in the BALF samples showed that the increases in cellular infiltrates in smoke-treated WT B6 mice were dominated by macrophages with an associated increase in neutrophils (Fig. 7*B*). In contrast, the numbers of macrophages and neutrophils in the BALFs of smoke-treated Prss31-null mice were not significantly different from the untreated animals (Fig. 7*B*). In agreement with these data, smoke-treated Prss31-null mice had reduced histopathology scores in their lungs compared with WT mice (Fig. 7, *C* and *D*).

Although exposure to cigarette smoke resulted in increased fibrosis around the small airways of WT mice as assessed histochemically (Fig. 7, *E* and *F*), this remodeling event was reduced in the lungs of smoke-treated Prss31-null mice. The lack of expression of Prss31 in the lungs of smoke-treated B6 mice did not affect resistance, dynamic compliance, tissue damping, or work of breathing. Nevertheless, smoke-treated Prss31-null mice had unchanged static compliance, in contrast to smoke-treated WT mice (Fig. 7*G*).

Experimental Acute Colitis—In support of the COPD data, DSS-induced acute colitis was significantly reduced in Prss31-

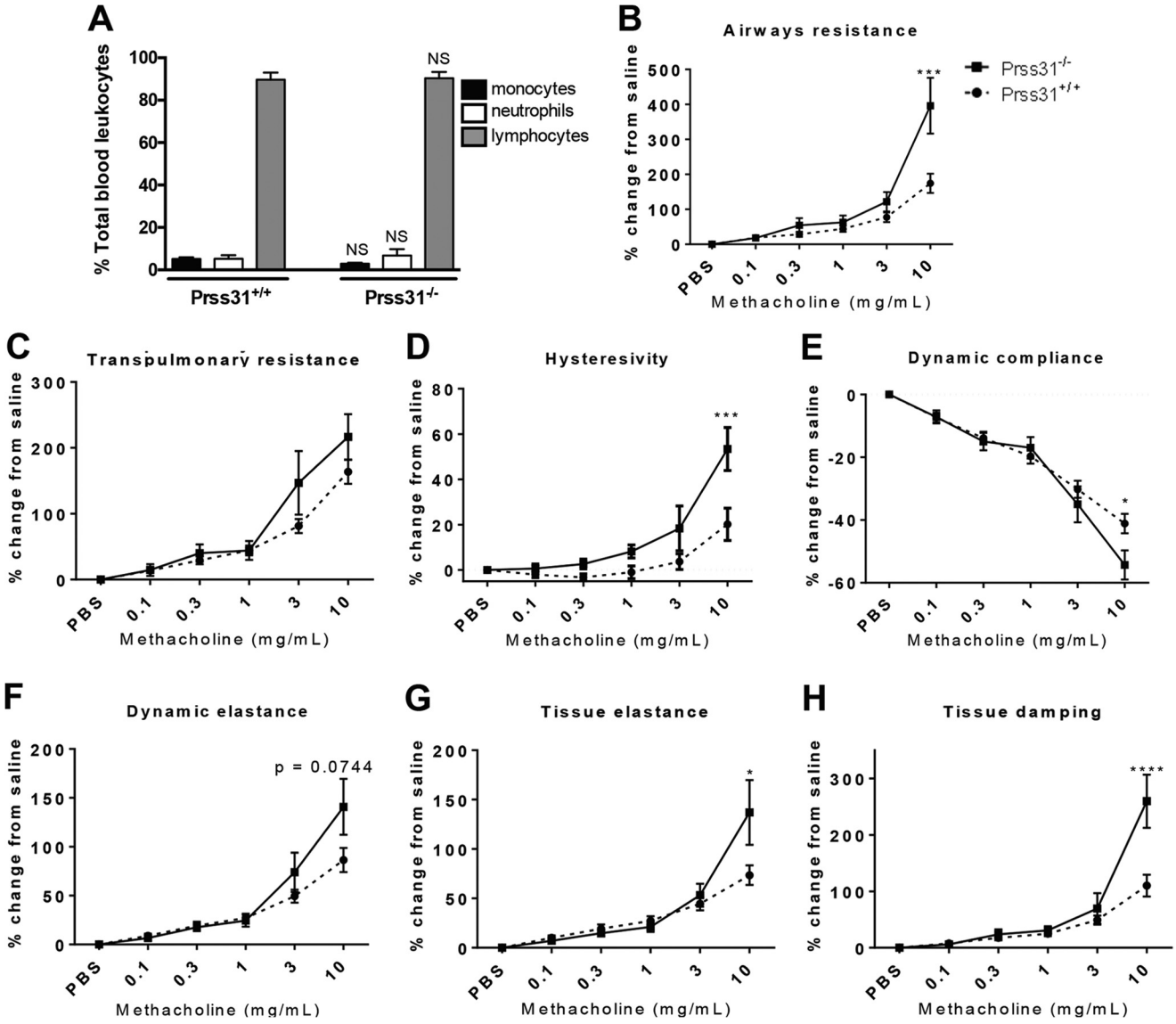

FIGURE 6. **Baseline blood cell populations and airway hyperresponsiveness to methacholine.** *A*, cardiac punctures were performed on naive WT and Prss31-null mice, and in each instance a single drop of blood was spread onto a microscope glass slide. Slides were stained with H&E and differential leukocyte counts were obtained based on cellular morphology. There were no differences in baseline blood cell populations between naive WT and Prss31-null mice. *B–H*, naive WT (●) and Prss31-null (■) B6 mice were cannulated and attached to a forced maneuver (Buxco) or oscillation (Flexivent) system, and lung function parameters were assessed. When on the forced oscillation system, the mice were challenged with 15-μl solutions containing 0–10 mg/ml methacholine. Relative to naive WT mice, the airways of naive Prss31-null mice were more responsive to the muscarinic receptor agonist. The latter transgenic mice had increased airway resistance (*B*), transpulmonary resistance (*C*), hysteresivity (*D*), dynamic elastance (*F*), tissue elastance (*G*), and tissue damping (*H*), as well as reduced dynamic compliance (*E*). The data are the mean ± S.E. of 6–8 mice. *A*, the *NS* above the compared columns corresponds to *p* values that were not significant. *B–H*, the *, ***, and **** symbols *above* curves correspond to *p* values that were <0.05, <0.001, and <0.0001, respectively.

null B6 mice relative to WT B6 mice (Fig. 8). Male age-matched and sibling WT and Prss31-null mice ingested 2% DSS in their drinking water for 5 days. On days 6 and 7, the two groups of mice were then given normal drinking water. The animals were sacrificed on day 7, which is when weight loss and inflammation are maximal after WT B6 mice are subjected to this acute colitis model. During the 7-day time period, Prss31-null B6 mice lost only 5.8 ± 0.6% ($n = 11$) of their original weight compared with WT B6 mice that lost 11.1 ± 1.3% ($n = 12$, $p < 0.01$) (Fig. 8*A*). At the time of sacrifice, the colons of these same DSS-treated WT mice were shortened to 6.6 ± 0.1 cm compared with the Prss31-null B6 mice colons that were 7.2 ± 0.1 cm ($p < 0.001$) (Fig. 8*B*). For comparison, the colons of the WT B6 and Prss31-null B6 mice that had not been exposed to DSS were 8.1 ± 0.2 and 8.0 ± 0.2 cm, respectively.

Histopathology scores were determined to assess the microscopic changes in DSS-induced colitis that correlated with the weight and colon length changes. A 20-point scoring system that incorporates six different categories of mucosal damage and inflammation was used. In these DSS experiments, there was a significant difference in the histopathology between the treated Prss31-null B6 mice that had a less severe 9.5 ± 0.8 histopathology score compared with DSS-treated WT mice that scored 14.5 ± 0.6 ($p < 0.0001$) (Fig. 8*C*). Representative images are depicted in Fig. 8*D* that demonstrate less epithelial cell crypt loss and inflammatory cell infiltrate in the colonic

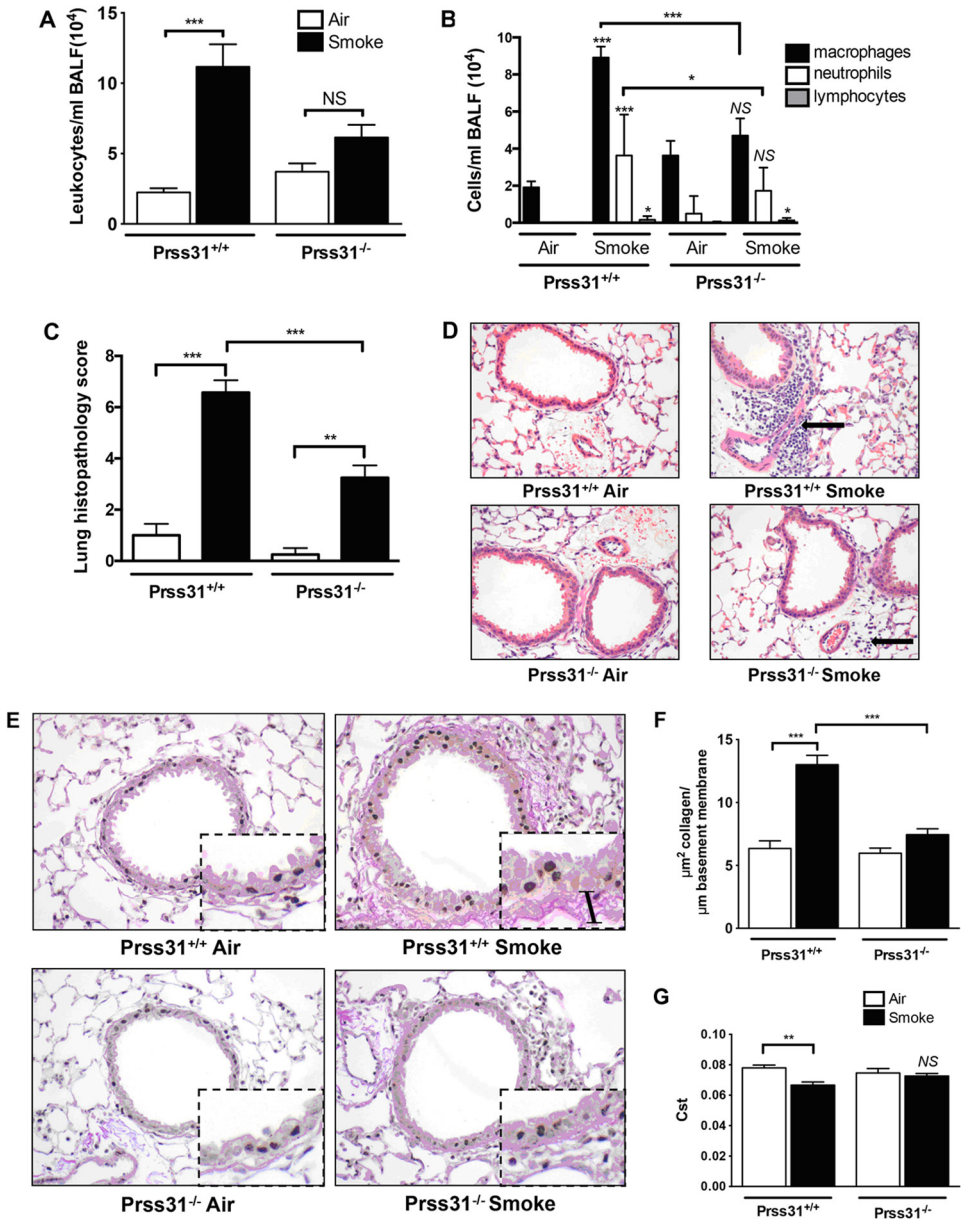

FIGURE 7. **Experimental COPD.** *A–G*, WT and Prss31-null B6 mice were exposed to cigarette smoke for 8 weeks. The BALF was collected in each instance, and cell counts and cytospins were performed to enumerate the numbers of total leukocytes, as well as the numbers of macrophages, neutrophils, and lymphocytes. Replicate lungs were perfused, inflated, paraffin-embedded, sectioned, and stained, and then histopathology scores were determined. Greater numbers of macrophages and neutrophils were found in the BALF of smoke-treated WT mice relative to smoke-treated Prss31-null mice (*A* and *B*). The histopathology scores (*C* and *D*) also were reduced in smoke-treated Prss31-null mice. The *black arrow* in the *upper right panel* of *D* highlights the inflammation in the lungs of smoke-treated WT mice. Baseline fibrosis (presumably collagen accumulation) in the small airways and lung function of the mice were then examined. As assessed histochemically (*E* and *F*), there was more fibrosis present in the small airways of smoke-treated WT mice (*bar* in the *inset* of the *upper right panel* of *E*) than in the lungs of smoke-treated Prss31-null mice (*E* and *F*). Although exposure of WT B6 mice to cigarette smoke for 8 weeks resulted in a reduced pulmonary static compliance (*Cst*) (*G*), this did not occur in similarly treated Prss31-null mice. The data are the mean ± S.E. of 6–8 mice. The *NS*, *, **, and *** symbols *above* the compared columns correspond to *p* values that were not significant or were <0.05, <0.01, and <0.001, respectively.

mucosa of DSS-treated Prss31-null relative to treated WT B6 mice.

In regard to the mechanism(s) by which Prss31 controls inflammation in the DSS-induced colitis model, no significant differences in the levels of the Mmp-13 and Cxcl-1 transcripts were found in the colons of DSS-treated WT and Prss31-null B6 mice (Fig. 9, *C* and *D*). Nevertheless, in support of the weight loss and histopathology data (Fig. 8), the levels of the transcripts that encode the pro-inflammatory cytokine IL-6 and the neutrophil-responsive chemokine Cxcl-2 were significantly lower in the colons of DSS-treated Prss31-null mice relative to that in the colons of DSS-treated WT mice (Fig. 9, *A* and *B*).

DISCUSSION

It has been known for >2 decades that the three tryptases present in the secretory granules of human and mouse MCs have redundant/overlapping enzymatic activities *in vitro*. Whether or not these *in vitro* data hold up *in vivo* can only be established by the creation of transgenic mice on a common genetic background that lack different combinations of these

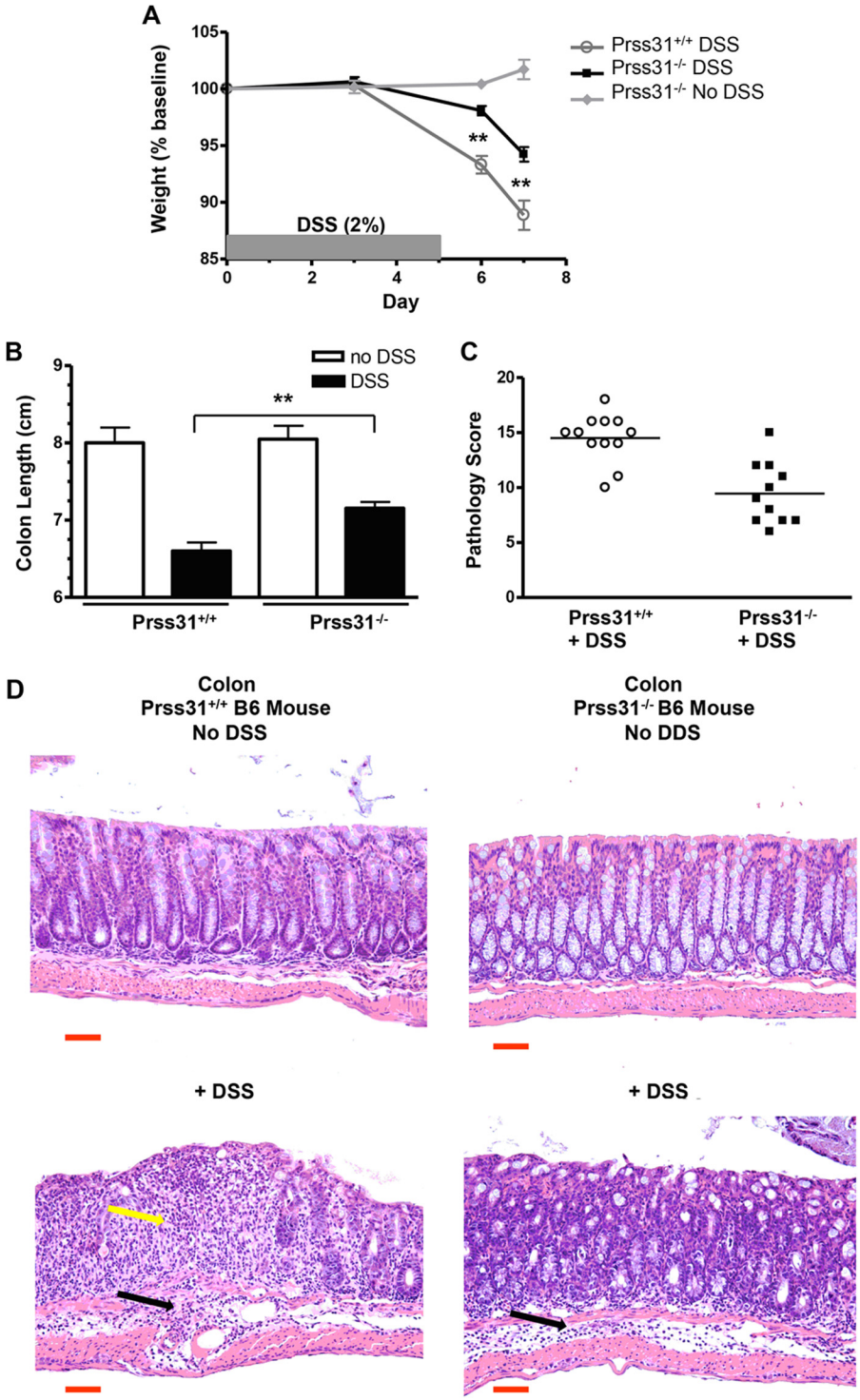

FIGURE 8. **Experimental colitis.** WT and Prss31-null mice were exposed to DSS for 7 days. WT (○) and age-matched Prss31-null (■ and ♦) B6 mice were untreated (♦) or were administered 2.0% DSS in their drinking water for 5 days, and then normal drinking water on days 6 and 7 (○ and ■). The resulting mice were sacrificed at day 7. Relative to DSS-treated WT mice, DSS-treated Prss31-null mice lost less weight (**, $p < 0.01$) (*A*), had longer colons (**, $p < 0.001$) (*B*), and lower histopathology scores ($p < 0.001$) (*C*). Assessed histochemically (*D*), more neutrophils and other inflammatory cells (*yellow arrow, bottom left panel*) accumulated in the mucosa of the colons of DSS-treated WT mice. However, the extent of inflammation of the submucosa and muscle layers of the DSS-treated Prss31-null and WT animals were similar (*black arrows*). For size comparison, the 50-μm magnification bar (*red*) is indicated in each panel of *D*.

enzymes. Using our previously created $6^{-}/7^{-}/31^{+}$ B6 mice (10), we discovered that the tetramer-forming tryptases mMCP-6 and mMCP-7 have similar *in vivo* bioactivities in blood coagulation (38, 39) and experimental arthritis (12). Because of the possibility that mMCP-7 and Prss31 also might have overlapping bioactivities *in vivo*, we concluded that it was imperative that we knock out the *Prss31* gene in mMCP-$7^{-/-}$ B6 mouse ES cells rather than in mMCP-$7^{+/+}$ 129/Sv or BALB/c mouse ES cells. Because that was done using our Cre/loxP homologous recombination approach (Fig. 1), the MCs in

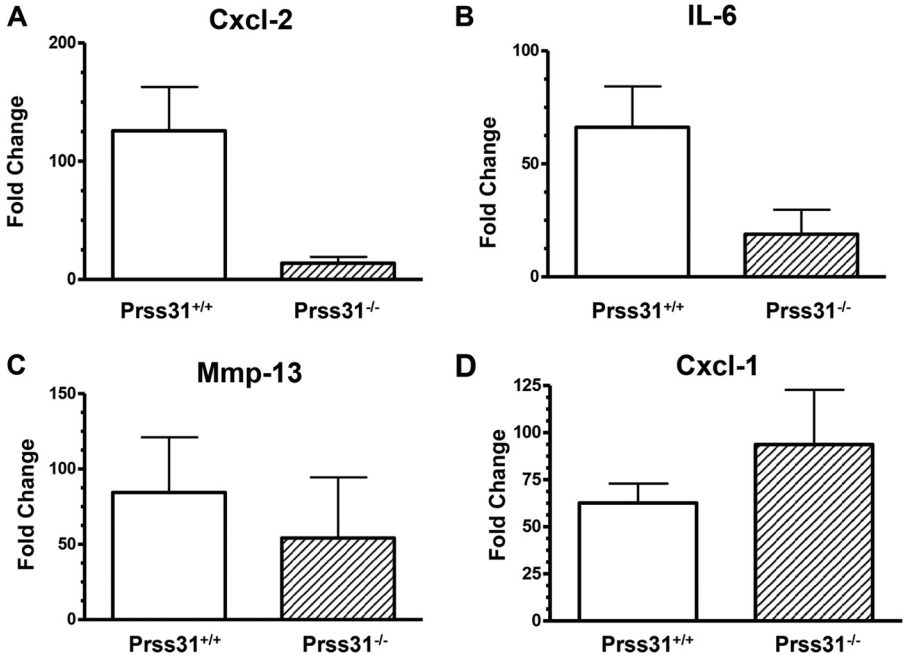

FIGURE 9. **Transcript levels in the colons of DSS-treated WT and Prss31-null B6 mice.** *A–D*, after colitis was induced in WT ($n = 5$) and Prss31$^{-/-}$ ($n = 5$) B6 mice, the two groups of animals were sacrificed, and RNA was isolated to evaluate the levels of the transcripts that encode Cxcl-2 (*A*), IL-6 (*B*), Mmp-13 (*C*), and Cxcl-1 (*D*). The obtained data were first normalized to those of the GAPDH transcript and then to untreated mice. In this colitis model, the colons of DSS-treated WT mice contained more Cxcl-2 ($p = 0.017$) and IL-6 ($p = 0.055$) mRNA than the colons of DSS-treated Prss31$^{-/-}$ mice. In contrast, the levels of the transcripts that encode Cxcl-1 and MMP-13 were not significantly different between the two groups of DSS-treated animals, in contrast to what occurs in DSS-treated mMCP-6-null mice.

lung and other connective tissues of our newly created mouse line have a $6^+/7^-/31^-$ tryptase phenotype.

WT BALB/c and 129/Sv mice constitutively lack Prss31 but express mMCP-7 (7). Thus, the MCs in the peritoneal cavity, skin, and other connective tissue sites of these two WT mouse strains have a $6^+/7^+/31^-$ tryptase phenotype. Because WT BALB/c, 129/Sv, and B6 mice are viable and have similar numbers of MCs in their tissues, it was known before we began our studies that Prss31 is not essential for the development of mice and their tissue MCs. We also showed in the 1990s (1, 2, 40, 41) that the MCs in the peritoneal cavity, skin, and other connective tissues of the WT $6^+/7^+/31^-$ BALB/c mouse contain large amounts of mMCP-4, mMCP-5, and mMCP-6 mRNA and protein. Thus, it also was known that the expression and granule accumulation of the latter three serine proteases in mouse peritoneal MCs are not dependent on Prss31.

Our newly created Prss31-null B6 mice were viable and had no obvious developmental abnormality in their MCs (Figs. 2–4). We therefore confirmed that Prss31 is not essential for the homing, retention, and overall granule maturation of the MCs that reside in varied tissues of the B6 mouse, including the granule storage of their other protease·serglycin proteoglycan complexes. As additionally anticipated, KitL-, IL-3-, IL-10-, IL-33-, and FcεRI-signaling pathways were intact in Prss31-null mouse MCs.

To deduce the *in vivo* function of Prss31, we evaluated the susceptibility of our newly created Prss31-null mice to methacholine. When our B6 mice were challenged with this synthetic choline ester, we discovered that Prss31 had a physiological protective function in the lung by minimizing airway responsiveness to the muscarinic receptor agonist (Fig. 6).

Our earlier discovery (14) that cigarette smoke-induced COPD was similar in WT $6^+/7^-/31^+$ B6 mice and WT $6^+/7^+/31^-$ BALB/c mice raised the possibility that mMCP-7 and Prss31 have similar bioactivities in this experimental disease. In support of that idea, cigarette smoke-induced experimental COPD was more pronounced in WT $6^+/7^-/31^+$ B6 mice compared with our newly created $6^+/7^-/31^-$ B6 mice (Fig. 7). This finding revealed for the first time that Prss31 has prominent adverse inflammatory roles in experimental COPD, as we previously showed for mMCP-6 (14). Humans who have inactivating mutations in the gene that encodes the serpin A1AT are at increased risk of developing emphysema even if they do not smoke (16), thereby documenting the importance of a A1AT/tryptic protease balance in the lungs. Although mMCP-6 and human tryptase-β are not susceptible to A1AT, we previously showed that recombinant human PRSS31 is rapidly inactivated by A1AT (7). The fact that the genetic loss of a natural inhibitor of Prss31 dramatically increases the risk of lung inflammation in humans supports our experimental mouse COPD data (Fig. 7).

We recently showed that mMCP-6 also has prominent adverse roles in DSS-induced colitis (13) and that this mouse ortholog of human tryptase-β acts upstream of many of the pathological factors in patients with inflammatory bowel disease. Prss31 is expressed early in developing MCs (42), and the intestine has the highest level of Prss31 mRNA in the body (4). We therefore evaluated the susceptibility of our Prss31-null B6 mice to DSS-induced colitis. In confirmation of the importance of Prss31 in a second MC-dependent inflammatory disease model, experimental colitis was significantly reduced in Prss31-null B6 mice relative to WT B6 mice (Fig. 8).

The discovery that the levels of the transcripts that encode the neutrophil-responsive chemokine Cxcl-2 and the pro-inflammatory cytokine IL-6 were both markedly reduced in the colons of DSS-treated Prss31-null B6 mice relative to treated WT B6 mice (Fig. 9) mechanistically explained, in part, why the accumulation of neutrophils was markedly reduced in the colons of the treated Prss31-null mice (Fig. 8*D*). Our data therefore provide new insights as to how MCs and specifically exocytosed tryptase Prss31 participate in inflammation and connective tissue remodeling in two very different disease models.

The mechanisms at the cellular level as to how Prss31 regulates baseline airway reactivity to methacholine, DSS-induced colitis, and cigarette smoke-induced COPD are likely to be complex, as we discovered for the tryptase's family members mMCP-6 and mMCP-7. Nevertheless, we previously showed that recombinant human PRSS31 could induce peripheral blood T cells and the Jurkat T cell line to quickly alter their expression of hundreds of transcripts *in vitro* (7). The putative receptor on the surfaces of T cells that is susceptible to human and mouse Prss31 remains to be identified. However, one possibility is a protease-activated receptor. All four of these signaling proteins are activated by tryptic proteases, and Jurkat cells express protease-activated receptors (43). In support of this hypothesis, protease-activated receptors have been implicated in airway responsiveness to methacholine (44) and in experimental colitis (45).

MMPs are the primary neutral proteases that participate in the remodeling of damaged connective tissue. Cigarette smoke-induced COPD is markedly attenuated in MMP-12-null mice (46), and lung remodeling was reduced in smoke-treated Prss31-null mice. That mMCP-6 and human tryptase-β can activate varied pro-MMPs (47–49) raises the additional possibility that Prss31 participates in remodeling of the smoke-damaged lung by activating pro-MMP-12 or another MMP zymogen.

Whatever mechanisms are operative in Prss31-dependent inflammation, it is now apparent that one must knock out at least two of the three tryptase genes in mouse MCs to uncover the prominent adverse activities of this family of serine proteases in experimental COPD and colitis. Because human MCs express three functionally similar tryptases encoded by the corresponding *TPSAB1, TPSB2*, and *TPSG1* genes, it is likely that the primary reason why the tryptase locus on human chromosome 16p13.3 has not been identified in genome-wide association studies of patients with COPD or inflammatory bowel disease is because of the *in vivo* redundancy of this family of MC-restricted serine proteases.

Approximately ~1.5 and ~13.5 million people in the United States alone have inflammatory bowel disease and COPD, respectively. Moreover, COPD is presently the third leading cause of death in the United States and carries an estimated ~2.1 trillion United States dollars yearly economic burden worldwide. Thus, there is a critical need to identify and fully understand novel inflammatory mediators and their pathways so that more effective pharmaceuticals can be developed. If our mouse data are relevant to what occurs in humans with COPD or colitis, the therapeutic potential of MC tryptase inhibitors may only be realized when both human tryptase-β and human PRSS31 are inactivated.

Acknowledgments—We thank Michael Gurish (Brigham and Women's Hospital) for the rabbit anti-mMCP-4 antibody used in the SDS-PAGE immunoblot analysis of lysates of MCs from WT and Prss31-null B6 mice. We also thank Kristy Wheeldon and Matthew Bowman for their technical assistance.

REFERENCES

1. Reynolds, D. S., Stevens, R. L., Lane, W. S., Carr, M. H., Austen, K. F., and Serafin, W. E. (1990) Different mouse mast cell populations express various combinations of at least six distinct mast cell serine proteases. *Proc. Natl. Acad. Sci. U.S.A.* **87,** 3230–3234
2. Reynolds, D. S., Gurley, D. S., Austen, K. F., and Serafin, W. E. (1991) Cloning of the cDNA and gene of mouse mast cell protease 6: transcription by progenitor mast cells and mast cells of the connective tissue subclass. *J. Biol. Chem.* **266,** 3847–3853
3. McNeil, H. P., Reynolds, D. S., Schiller, V., Ghildyal, N., Gurley, D. S., Austen, K. F., and Stevens, R. L. (1992) Isolation, characterization, and transcription of the gene encoding mouse mast cell protease 7. *Proc. Natl. Acad. Sci. U.S.A.* **89,** 11174–11178
4. Wong, G. W., Tang, Y., Feyfant, E., Sali, A., Li, L., Li, Y., Huang, C., Friend, D. S., Krilis, S. A., and Stevens, R. L. (1999) Identification of a new member of the tryptase family of mouse and human mast cell proteases that possesses a novel C-terminal hydrophobic extension. *J. Biol. Chem.* **274,** 30784–30793
5. Caughey, G. H., Raymond, W. W., Blount, J. L., Hau, L. W., Pallaoro, M., Wolters, P. J., and Verghese, G. M. (2000) Characterization of human γ tryptases, novel members of the chromosome 16p mast cell tryptase and prostasin gene families. *J. Immunol.* **164,** 6566–6575
6. Hunt, J. E., Stevens, R. L., Austen, K. F., Zhang, J., Xia, Z., and Ghildyal, N. (1996) Natural disruption of the mouse mast cell protease 7 gene in the C57BL/6 mouse. *J. Biol. Chem.* **271,** 2851–2855
7. Wong, G. W., Foster, P. S., Yasuda, S., Qi, J. C., Mahalingam, S., Mellor, E. A., Katsoulotos, G., Li, L., Boyce, J. A., Krilis, S. A., and Stevens, R. L. (2002) Biochemical and functional characterization of human transmembrane tryptase (TMT)/tryptase γ: TMT is an exocytosed mast cell protease that induces airway hyperresponsiveness *in vivo* via an IL-13/IL-4Rα/STAT6-dependent pathway. *J. Biol. Chem.* **277,** 41906–41915
8. Yuan, J., Beltman, J., Gjerstad, E., Nguyen, M. T., Sampang, J., Chan, H., Janc, J. W., and Clark, J. M. (2006) Expression and characterization of recombinant γ-tryptase. *Protein Expr. Purif.* **49,** 47–54
9. Huang, C., De Sanctis, G. T., O'Brien, P. J., Mizgerd, J. P., Friend, D. S., Drazen, J. M., Brass, L. F., and Stevens, R. L. (2001) Evaluation of the substrate specificity of human mast cell tryptase β1 and demonstration of its importance in bacterial infections of the lung. *J. Biol. Chem.* **276,** 26276–26284
10. Thakurdas, S. M., Melicoff, E., Sansores-Garcia, L., Moreira, D. C., Petrova, Y., Stevens, R. L., and Adachi, R. (2007) The mast cell-restricted tryptase mMCP-6 has a critical immunoprotective role in bacterial infections. *J. Biol. Chem.* **282,** 20809–20815
11. Shin, K., Watts, G. F., Oettgen, H. C., Friend, D. S., Pemberton, A. D., Gurish, M. F., and Lee, D. M. (2008) Mouse mast cell tryptase mMCP-6 is a critical link between adaptive and innate immunity in the chronic phase of *Trichinella spiralis* infection. *J. Immunol.* **180,** 4885–4891
12. McNeil, H. P., Shin, K., Campbell, I. K., Wicks, I. P., Adachi, R., Lee, D. M., and Stevens, R. L. (2008) The mouse mast cell-restricted tetramer-forming tryptases mouse mast cell protease 6 and mouse mast cell protease 7 are critical mediators in inflammatory arthritis. *Arthritis Rheum.* **58,** 2338–2346
13. Hamilton, M. J., Sinnamon, M. J., Lyng, G. D., Glickman, J. N., Wang, X., Xing, W., Krilis, S. A., Blumberg, R. S., Adachi, R., Lee, D. M., and Stevens, R. L. (2011) Essential role for mast cell tryptase in acute experimental colitis. *Proc. Natl. Acad. Sci. U.S.A.* **108,** 290–295
14. Beckett, E. L., Stevens, R. L., Jarnicki, A. G., Kim, R. Y., Hanish, I., Hansbro, N. G., Deane, A., Keely, S., Horvat, J. C., Yang, M., Oliver, B. G., van Rooijen, N., Inman, M. D., Adachi, R., Soberman, R. J., Hamadi, S., Wark, P. A., Foster, P. S., and Hansbro, P. M. (2013) A new short-term mouse

model of chronic obstructive pulmonary disease identifies a role for mast cell tryptase in pathogenesis. *J. Allergy Clin. Immunol.* **131,** 752–762
15. Keely, S., Talley, N. J., and Hansbro, P. M. (2012) Pulmonary-intestinal cross-talk in mucosal inflammatory disease. *Mucosal. Immunol.* **5,** 7–18
16. Cohen, B. H., Ball, W. C., Jr., Brashears, S., Diamond, E. L., Kreiss, P., Levy, D. A., Menkes, H. A., Permutt, S., and Tockman, M. S. (1977) Risk factors in chronic obstructive pulmonary disease (COPD). *Am. J. Epidemiol.* **105,** 223–232
17. Poller, W., Barth, J., and Voss, B. (1989) Detection of an alteration of the α2-macroglobulin gene in a patient with chronic lung disease and serum α2-macroglobulin deficiency. *Hum. Genet.* **83,** 93–96
18. Kitamura, Y., Go, S., and Hatanaka, K. (1978) Decrease of mast cells in W/W^v mice and their increase by bone marrow transplantation. *Blood* **52,** 447–452
19. Morii, E., Ogihara, H., Oboki, K., Kataoka, T. R., Jippo, T., and Kitamura, Y. (2001) Effect of MITF on transcription of transmembrane tryptase gene in cultured mast cells of mice. *Biochem. Biophys. Res. Commun.* **289,** 1243–1246
20. Chen, Y., Lu, J., Pan, H., Zhang, Y., Wu, H., Xu, K., Liu, X., Jiang, Y., Bao, X., Yao, Z., Ding, K., Lo, W. H., Qiang, B., Chan, P., Shen, Y., and Wu, X. (2003) Association between genetic variation of CACNA1H and childhood absence epilepsy. *Ann. Neurol.* **54,** 239–243
21. Chen, C. C., Lamping, K. G., Nuno, D. W., Barresi, R., Prouty, S. J., Lavoie, J. L., Cribbs, L. L., England, S. K., Sigmund, C. D., Weiss, R. M., Williamson, R. A., Hill, J. A., and Campbell, K. P. (2003) Abnormal coronary function in mice deficient in α1H T-type Ca^{2+} channels. *Science* **302,** 1416–1418
22. Ghildyal, N., Friend, D. S., Freelund, R., Austen, K. F., McNeil, H. P., Schiller, V., and Stevens, R. L. (1994) Lack of expression of the tryptase mouse mast cell protease 7 in mast cells of the C57BL/6J mouse. *J. Immunol.* **153,** 2624–2630
23. Enerbäck, L. (1966) Mast cells in rat gastrointestinal mucosa. 2. Dye-binding and metachromatic properties. *Acta Pathol. Microbiol. Scand.* **66,** 303–312
24. Friend, D. S., Ghildyal, N., Austen, K. F., Gurish, M. F., Matsumoto, R., and Stevens, R. L. (1996) Mast cells that reside at different locations in the jejunum of mice infected with *Trichinella spiralis* exhibit sequential changes in their granule ultrastructure and chymase phenotype. *J. Cell Biol.* **135,** 279–290
25. Razin, E., Ihle, J. N., Seldin, D., Mencia-Huerta, J. M., Katz, H. R., LeBlanc, P. A., Hein, A., Caulfield, J. P., Austen, K. F., and Stevens, R. L. (1984) Interleukin-3: a differentiation and growth factor for the mouse mast cell that contains chondroitin sulfate E proteoglycan. *J. Immunol.* **132,** 1479–1486
26. Ghildyal, N., Friend, D. S., Nicodemus, C. F., Austen, K. F., and Stevens, R. L. (1993) Reversible expression of mouse mast cell protease 2 mRNA and protein in cultured mast cells exposed to IL-10. *J. Immunol.* **151,** 3206–3214
27. Forsberg, E., Pejler, G., Ringvall, M., Lunderius, C., Tomasini-Johansson, B., Kusche-Gullberg, M., Eriksson, I., Ledin, J., Hellman, L., and Kjellén, L. (1999) Abnormal mast cells in mice deficient in a heparin-synthesizing enzyme. *Nature* **400,** 773–776
28. McNeil, H. P., Frenkel, D. P., Austen, K. F., Friend, D. S., and Stevens, R. L. (1992) Translation and granule localization of mouse mast cell protease 5: immunodetection with specific antipeptide Ig. *J. Immunol.* **149,** 2466–2472
29. Galli, S. J., Gordon, J. R., and Wershil, B. K. (1993) Mast cell cytokines in allergy and inflammation. *Agents Actions Suppl.* **43,** 209–220
30. Razin, E., Mencia-Huerta, J. M., Lewis, R. A., Corey, E. J., and Austen, K. F. (1982) Generation of leukotriene C_4 from a subclass of mast cells differentiated *in vitro* from mouse bone marrow. *Proc. Natl. Acad. Sci. U.S.A.* **79,** 4665–4667
31. Robinson, D., and Stirling, J. L. (1968) *N*-Acetyl-β-glucosaminidases in human spleen. *Biochem. J.* **107,** 321–327
32. Essilfie, A. T., Simpson, J. L., Horvat, J. C., Preston, J. A., Dunkley, M. L., Foster, P. S., Gibson, P. G., and Hansbro, P. M. (2011) *Haemophilus influenzae* infection drives IL-17-mediated neutrophilic allergic airways disease. *PLoS Pathog.* **7,** e1002244
33. Horvat, J. C., Beagley, K. W., Wade, M. A., Preston, J. A., Hansbro, N. G., Hickey, D. K., Kaiko, G. E., Gibson, P. G., Foster, P. S., and Hansbro, P. M. (2007) Neonatal chlamydial infection induces mixed T-cell responses that drive allergic airway disease. *Am. J. Respir. Crit. Care Med.* **176,** 556–564
34. Horvat, J. C., Starkey, M. R., Kim, R. Y., Phipps, S., Gibson, P. G., Beagley, K. W., Foster, P. S., and Hansbro, P. M. (2010) Early-life chlamydial lung infection enhances allergic airways disease through age-dependent differences in immunopathology. *J. Allergy Clin. Immunol.* **125,** 617–625
35. Fricker, M., Deane, A., and Hansbro, P. M. (2014) Animal modes of chronic obstructive pulmonary disease. *Expert Opin. Drug Discov.* **9,** 629–645
36. Okayasu, I., Hatakeyama, S., Yamada, M., Ohkusa, T., Inagaki, Y., and Nakaya, R. (1990) A novel method in the induction of reliable experimental acute and chronic ulcerative colitis in mice. *Gastroenterology* **98,** 694–702
37. Garrett, W. S., Lord, G. M., Punit, S., Lugo-Villarino, G., Mazmanian, S. K., Ito, S., Glickman, J. N., and Glimcher, L. H. (2007) Communicable ulcerative colitis induced by T-bet deficiency in the innate immune system. *Cell* **131,** 33–45
38. Huang, C., Wong, G. W., Ghildyal, N., Gurish, M. F., Sali, A., Matsumoto, R., Qiu, W. T., and Stevens, R. L. (1997) The tryptase, mouse mast cell protease 7, exhibits anticoagulant activity *in vivo* and *in vitro* due to its ability to degrade fibrinogen in the presence of the diverse array of protease inhibitors in plasma. *J. Biol. Chem.* **272,** 31885–31893
39. Prieto-García, A., Zheng, D., Adachi, R., Xing, W., Lane, W. S., Chung, K., Anderson, P., Hansbro, P. M., Castells, M., and Stevens, R. L. (2012) Mast cell restricted mouse and human tryptase-heparin complexes hinder thrombin-induced coagulation of plasma and the generation of fibrin by proteolytically destroying fibrinogen. *J. Biol. Chem.* **287,** 7834–7844
40. McNeil, H. P., Austen, K. F., Somerville, L. L., Gurish, M. F., and Stevens, R. L. (1991) Molecular cloning of the mouse mast cell protease 5 gene: a novel secretory granule protease expressed early in the differentiation of serosal mast cells. *J. Biol. Chem.* **266,** 20316–20322
41. Serafin, W. E., Sullivan, T. P., Conder, G. A., Ebrahimi, A., Marcham, P., Johnson, S. S., Austen, K. F., and Reynolds, D. S. (1991) Cloning of the cDNA and gene for mouse mast cell protease 4: demonstration of its late transcription in mast cell subclasses and analysis of its homology to subclass-specific neutral proteases of the mouse and rat. *J. Biol. Chem.* **266,** 1934–1941
42. Wong, G. W., Yasuda, S., Morokawa, N., Li, L., and Stevens, R. L. (2004) Mouse chromosome 17A3.3 contains 13 genes that encode functional tryptic-like serine proteases with distinct tissue and cell expression patterns. *J. Biol. Chem.* **279,** 2438–2452
43. Bar-Shavit, R., Maoz, M., Yongjun, Y., Groysman, M., Dekel, I., and Katzav, S. (2002) Signalling pathways induced by protease-activated receptors and integrins in T cells. *Immunology* **105,** 35–46
44. De Campo, B. A., and Henry, P. J. (2005) Stimulation of protease-activated receptor-2 inhibits airway eosinophilia, hyperresponsiveness and bronchoconstriction in a murine model of allergic inflammation. *Br. J. Pharmacol.* **144,** 1100–1108
45. Fiorucci, S., Mencarelli, A., Palazzetti, B., Distrutti, E., Vergnolle, N., Hollenberg, M. D., Wallace, J. L., Morelli, A., and Cirino, G. (2001) Proteinase-activated receptor 2 is an anti-inflammatory signal for colonic lamina propria lymphocytes in a mouse model of colitis. *Proc. Natl. Acad. Sci. U.S.A.* **98,** 13936–13941
46. Hautamaki, R. D., Kobayashi, D. K., Senior, R. M., and Shapiro, S. D. (1997) Requirement for macrophage elastase for cigarette smoke-induced emphysema in mice. *Science* **277,** 2002–2004
47. Magarinos, N. J., Bryant, K. J., Fosang, A. J., Adachi, R., Stevens, R. L., and McNeil, H. P. (2013) Mast cell-restricted, tetramer-forming tryptases induce aggrecanolysis in articular cartilage by activating matrix metalloproteinase-3 and -13 zymogens. *J. Immunol.* **191,** 1404–1412
48. Gruber, B. L., Schwartz, L. B., Ramamurthy, N. S., Irani, A. M., and Marchese, M. J. (1988) Activation of latent rheumatoid synovial collagenase by human mast cell tryptase. *J. Immunol.* **140,** 3936–3942
49. Gruber, B. L., Marchese, M. J., Suzuki, K., Schwartz, L. B., Okada, Y., Nagase, H., and Ramamurthy, N. S. (1989) Synovial procollagenase activation by human mast cell tryptase dependence upon matrix metalloproteinase 3 activation. *J. Clin. Invest.* **84,** 1657–1662